Title

A true multi-modality approach for high resolution optical imaging: photo-magnetic imaging

Permalink

https://escholarship.org/uc/item/3fv9782p

Authors

Luk, Alex T
Ha, Seunghoon
Nouizi, Farouk
et al.

Publication Date

2014-02-17

DOI

10.1117/12.2040870

Peer reviewed

A True Multi-modality Approach for High Resolution Optical Imaging: Photo-Magnetic Imaging

Alex T. Luk[1], **Seunghoon Ha**[1], **Farouk Nouizi**[1], **David Thayer**[1], **Yuting Lin**[1], and **Gultekin Gulsen**[1,2]

[1]Tu and Yuen Center for Functional Onco-Imaging and Department of Radiological Sciences, University of California Irvine, Irvine, CA, United States

[2]Department of Biomedical Engineering, University of California Irvine, California 92697

Abstract

Multi-modality imaging leverages the competitive advantage of different imaging systems to improve the overall resolution and quantitative accuracy. Our new technique, Photo-Magnetic Imaging (PMI) is one of these true multi-modality imaging approaches, which can provide quantitative optical absorption map at MRI spatial resolution. PMI uses laser light to illuminate tissue and elevate its temperature while utilizing MR thermometry to measure the laser-induced temperature variation with high spatial resolution. The high-resolution temperature maps are later converted to tissue absorption maps by a finite element based inverse solver that is based on modeling of photon migration and heat diffusion in tissue. Previously, we have demonstrated the feasibility of PMI with phantom studies. Recently, we have managed to reduce the laser power under ANSI limit for maximum skin exposure therefore, we have well positioned PMI for *in vivo* imaging. Currently we are expanding our system by adding multi-wavelength imaging capability. This will allow us not only to resolve spatial distribution of tissue chromophores but also exogenous contrast agents. Although we test PMIs feasibility with animal studies, our future goal is to use PMI for breast cancer imaging due to its high translational potential.

Keywords

Photo-magnetic Imaging; Diffuse Optical Tomography; MRI; Thermography; High Resolution; Quantitative Accuracy

1. INTRODUCTION

Comparing to other anatomical imaging modalities such as Magnetic Resonance Imaging (MRI), X-ray CT and ultrasound, diffuse optical imaging can provide functional information about bio tissue. However, it suffers from low resolution and low quantity accuracy. In recent years, many research groups have spent extensive effort to improve the quality of the diffuse optical imaging. One particular approach is using *a priori* anatomical information acquired by another high-resolution imaging modality like X-ray CT or MRI to guide and

constrain the image reconstruction process to increase the accuracy. However, there is an intrinsic problem in diffuse optical imaging: the signals are only detected from the boundary of the medium. Using these 2D measurements, diffuse optical imaging aims to render 3D optical property maps from the whole volume. Unfortunately, high scattering nature of the tissue, makes the inverse problem very challenging and results in poor resolution and low spatial resolution. Multi-modality approach is proven to be an effective way to improve the optical imaging performance [1–4]. Meanwhile, the combination of optical and ultrasound techniques has led the development of photo-acoustic tomography (PAT), which can also provide the functional information such as hemoglobin concentration and visualize exogenous contrast agents as well as molecular and functional markers with high resolution. PAT takes advantage of the relatively low scattering nature of the acoustic wave to overcome the resolution limit of the diffuse optical tomography but unfortunately, its resolution degrades with depth drastically [5–8]. Here we propose a new multimodality optical imaging technique termed photo-magnetic imaging (PMI), which replaces optical detectors with the MRI. The novelty of PMI is utilization of MRI to measure the temperature increase induced by the near infrared light, which is correlated with the photon density at a particular region and local optical absorption. MRI can measure the temperature from the whole 3D volume of the probed medium. Each voxel of MR Thermography image will act as a temperature detector at that particular position. Using finite element method (FEM) to model the photon propagation and heat generation/diffusion in tissue, we can solve the PMI inverse problem: rendering the tissue optical absorption map with high resolution and high accuracy from the MRI high resolution temperature map. The PMI solves the intrinsic problem of conventional diffuse optical imaging by increasing the dimension of optical measurements from 2D to 3D.

2. METHODS

There are many MR thermometry techniques available [9–13]. Proton resonant frequency (PRF), the diffusion coefficient, T1 and T2 relaxation time, magnetization transfer, proton density are the parameters changing with the temperature of the medium. Using different MRI sequence, one can measure the change of these parameter which correspond to the difference of the temperature. Considering sensitivity, linearity, the ability to make absolute or relative measurements, acquisition time, tissue type specificity and sensitivity to artifacts and our measured target, proton resonance frequency shift method is one of the best options.

Proton resonance frequency changes with the tissue temperature which results in different MRI phase signal with same MRI echo time. We can use normal MRI gradient echo sequence to acquire the phase map of the medium to calculate the temperature difference of the medium. This method has been widely used and has the advantage of fast speed, high spatial resolution and high temperature sensitivity [14, 15].]. Figure 1. shows a linear relationship between the MRI gradient echo sequence phase signal and temperature. A 100 cm diameter Agar phantom has been cooled down in the refrigerator and then positioned in the center of the MRI scanner. The agar phantom warmed up approximately 3 degrees over a period of 30 minutes due to the MRI scanner room temperature. We acquired MRI measurement during this period with a MR compatible fiber optic temperature probe to

record the phantom temperature at the same time. The figure shows that the accuracy of MRI was nearly +/− 0.05C°.

The hydrogen procession speed is linear proportion to the medium temperature. The speed difference of the medium with different temperature will result in a phase difference which will also have a linear relationship with the temperature difference as described by Equation 1. Here, γ is gyromagnetic frequency of hydrogen atom (42.5Mhz). Alpha is proton resonance frequency shift constant. B0 is the magnetic field. In our center, we are using 3Tesla Philips Achieva system. TE is the echo time of the MRI gradient echo sequence.

$$\Delta T = \frac{\Delta \theta(T)}{\gamma \cdot \alpha \cdot B0 \cdot TE} \quad (1)$$

For PMI data analysis, we use the diffusion approximation to model the photon propagation and bio-heat equation to model heat transfer in the tissue. PMI is the first-of-its-kind MR and optical imaging combination, in which both work in harmonic together. We use finite element method (FEM) to solve both equations in a coupled manner [16–18]. Equation 2 is the steady-state representation of the optical diffusion equation [19]. φ(r) is the optical light fluence rate (W.mm^{-2}), s(r) is the optical light source (W.mm^{-3}), D(r) is the photon diffusion coefficient, μa is the photon absorption coefficient of the medium. Equation 3 is the bio-heat equation [20, 21], ρ, c, and k denotes density, specific heat, and thermal conductivity of tissue; c_b is the specific heat of blood and w_b is blood perfusion rate. Q_R is the imposed spatial heating induced by near infrared laser. Q_M is the metabolic heat generation. T_a is the supplying arterial blood temperature and T is the tissue temperature. Please note that in our phantom studies, we neglect the metabolic heat generation and heat sink term due to local blood supply.

$$\overrightarrow{\nabla}.D(\overrightarrow{r})\overrightarrow{\nabla}\phi(\overrightarrow{r}) - \mu_a(\overrightarrow{r})\phi(\overrightarrow{r}) = -S(\overrightarrow{r}) \quad (2)$$

$$\rho.c.\frac{\partial T(\overrightarrow{r},t)}{\partial t} = \nabla k \nabla T(\overrightarrow{r},t) + Q_R + Q_M + w_b.c_b(T_a(\overrightarrow{r},t) - T(\overrightarrow{r},t)) \quad (3)$$

Figure 2. shows the PMI set-up. Four ten meters long optical fibers are used to transfer light from MRI control room. The fibers are coupled into a specially designed MRI coil, which can illuminate the medium from four sides as shown in the figure. The laser light is collimated with aspherecial lenses (Newport, CA) to illuminate the medium. The PMI interface coil is positioned at the center of the MRI bore during scanning. Figure 3. shows the timing diagram of PMI.

We have measured the phase difference between the heating and baseline MRI maps to determine the phase change corresponding to the laser-induced temperature change. Using Equation 1, we can convert the phase difference map into a relative temperature map of the subject. The temperature map can be further used to obtain the optical absorption distribution using FEM inverse solver and Equations 2&3. The number of heating phase

scans depends on the study purpose. For example, if the PMI is used for dynamic imaging (e.g. measuring pharmacokinetics of an optical contrast agent) multiple MRI measurements are performed during the heating phase. Figure 4. shows the PMI coil during baseline phase (laser is off) and heating phase (laser is on) scans. PMI coil is connected to a four-channel MRI compatible amplifier box to increase the signal prior to the MRI scanner receiver unit. Figure 4.b is captured using a SONY night vision camera to depict near infrared laser light emitted from four laser probes. The laser wavelength is 808nm and selected for optimum penetration in tissue. MRI field of view is 60 mm × 60 mm. TR time is 50 ms. TE time is set to 8 ms,12 ms and 16 ms. Scanning time for each MRI slice is 5 to 20 seconds depending on the selected image resolution.

3. RESULTS

A circular agar phantom embedded with a high absorption inclusion is used to demonstrate the high resolution and quantity accuracy of PMI system. Here we use a gradient index lens in front of the optical fiber to collimate the laser beam. The agar phantom is mixed with optical dye. The absorption coefficient of the phantom is set to 0.01mm^{-1}. The absorption coefficient of the embedded inclusion is four times higher than the background, 0.04 mm^{-1}. The phantom design, the true absorption map of the phantom, is given in Figure 5.a. Using FEM based forward model that we have developed in our lab, we simulate the photon distribution after we turn on the laser. The photon distribution has been shown in Figure 5.c in log scale. As we expected, the embedded high absorption inclusion area absorbs more photons and decreases the photon density around the inclusion. The energy deposited to the phantom by the optical photons increases the temperature of the phantom. The high absorption inclusion absorbs more photons, therefore the temperature increase in that area is higher than the background. Figure 5.d and Figure 5.e show that the temperature distribution obtained by MR thermometry at two different time points of the heating phase scan.

We also use the FEM based forward model to simulate the bio-heat equation and obtain a simulated temperature map of the phantom to compare with the real MRI measurement. Figure 6.a shows the temperature map generated by the FEM based forward model. Figure 6.b is the temperature map of the phantom measured by the PMI system. The profile across the center of the phantom and the embedded inclusion for both temperature maps match to each other and confirms our modelling.

4. CONCLUSION

Photo-Magnetic Imaging (PMI) can provide quantitative optical absorption maps at MRI spatial resolution. It uses laser light to illuminate the tissue and elevate the temperature while utilize MR thermometry to measure the laser induced temperature variation with high spatial resolution. The high resolution temperature maps are later converted to tissue absorption maps by a finite element based inverse solver that utilize modeling of photon migration and heat diffusion in tissue. We have also shown that the accuracy of the PMI modeling through comparison of forward simulation and MR thermometry measurements. We believe that with the ability to perform whole body imaging of small animals in vivo, PMI will be a very powerful tool to help the development of optical molecular probes.

Furthermore, it can also enhance the role of the MRI from diagnosis to the therapy planning and monitoring of cancer by providing additional complementary functional information.

ACKNOWLEDGEMENT

REFERENCES

1. Lin Y, Ghijsen MT, Gao H, Liu N, Nalcioglu O, Gulsen G. A photo-multiplier tube-based hybrid MRI and frequency domain fluorescence tomography system for small animal imaging. Phys Med Biol. 2011; 56:4731–4747. [PubMed: 21753235]

2. Unlu MB, Lin Y, Birgul O, Nalcioglu O, Gulsen G. Simultaneous in vivo dynamic magnetic resonance-diffuse optical tomography for small animal imaging. J Biomed Opt. 2008; 13:060501. [PubMed: 19123642]

3. Gulsen G, Birgul O, Unlu MB, Shafiiha R, Nalcioglu O. Combined diffuse optical tomography (DOT) and MRI system for cancer imaging in small animals. Technol Cancer Res Treat. 2006; 5:351–363. [PubMed: 16866566]

4. Lin WBY, Iwanczyk J, Roeck W, Nalcioglu O, Gulsen G. Quantitative fluorescence tomography using a combined tri-modality FT/DOT/XCT system. Optics Express. 2010; 18:7835–7850. [PubMed: 20588625]

5. Yuan Z, Jiang H. Quantitative photoacoustic tomography. Philos Transact A Math Phys Eng Sci. 2009; 367:3043–3054.

6. Stein EW, Maslov K, Wang LV. Noninvasive, in vivo imaging of blood-oxygenation dynamics within the mouse brain using photoacoustic microscopy. J Biomed Opt. 2009; 14:020502. [PubMed: 19405708]

7. Wang LV. Multiscale photoacoustic microscopy and computed tomography. Nat Photon. 2009; 3:503–509.

8. T K, A C, M L, L H, M R, M K, Ermilov T, A S, Oraevsky AA. Laser optoacoustic imaging system for detection of breast cancer. J. Biomed. Opt. 2009; 14:024007. [PubMed: 19405737]

9. Kim JH, Hahn EW. Clinical and biological studies of localized hyperthermia. Cancer Res. 1979; 39:2258–2261. [PubMed: 445426]

10. Chen J, Daniel BL, Pauly KB. Investigation of proton density for measuring tissue temperature. J Magn Reson Imaging. 2006; 23:430–434. [PubMed: 16463298]

11. Bottomley PA, Foster TH, Argersinger RE, Pfeifer LM. A review of normal tissue hydrogen NMR relaxation times and relaxation mechanisms from 1–100 MHz: dependence on tissue type, NMR frequency, temperature, species, excision, and age. Med Phys. 1984; 11:425–448. [PubMed: 6482839]

12. De Poorter J, De Wagter C, De Deene Y, Thomsen C, Stahlberg F, Achten E. Noninvasive MRI thermometry with the proton resonance frequency (PRF) method: in vivo results in human muscle. Magn Reson Med. 1995; 33:74–81. [PubMed: 7891538]

13. Graham SJ, Stanisz GJ, Kecojevic A, Bronskill MJ, Henkelman RM. Analysis of changes in MR properties of tissues after heat treatment. Magn Reson Med. 1999; 42:1061–1071. [PubMed: 10571927]

14. Ishihara Y, Calderon A, Watanabe H, Okamoto K, Suzuki Y, Kuroda K. A precise and fast temperature mapping using water proton chemical shift. Magn Reson Med. 1995; 34:814–823. [PubMed: 8598808]

15. Rieke V, Butts Pauly K. MR thermometry. J Magn Reson Imaging. 2008; 27:376–390. [PubMed: 18219673]

16. BO Unlu BM, Shafihaa R, Gulsen G, Nalcioglu O. Diffuse Optical Tomographic Reconstruction Using Multi-frequency Data. J Biomed Opt. 2006; 11:054008. [PubMed: 17092157]

17. Lin Y, et al. Fluorescence diffuse optical tomography with functional and anatomical a priori information: feasibility study. Physics in Medicine and Biology. 2007; 52:5569. [PubMed: 17804882]

18. Lin Y, Yan H, Nalcioglu O, Gulsen G. Quantitative fluorescence tomography with functional and structural a priori information. Appl Opt. 2009; 48:1328–1336. [PubMed: 19252634]

19. Arridge SR. Optical tomography in medical imaging. Inv. Prob. 1999; 15:R41.

20. CU Tunc M, Parmaksizoglu C, Ciriksi S. The bio-heat transfer equation and its applications in hyperthermia treatments. Intenational Journal of Computer Aided Engineering and Software. 2006; 23:451–453.

21. Crezee J, Mooibroek J, Lagendijk JJ, van Leeuwen GM. The theoretical and experimental evaluation of the heat balance in perfused tissue. Phys Med Biol. 1994; 39:813–832. [PubMed: 15552087]
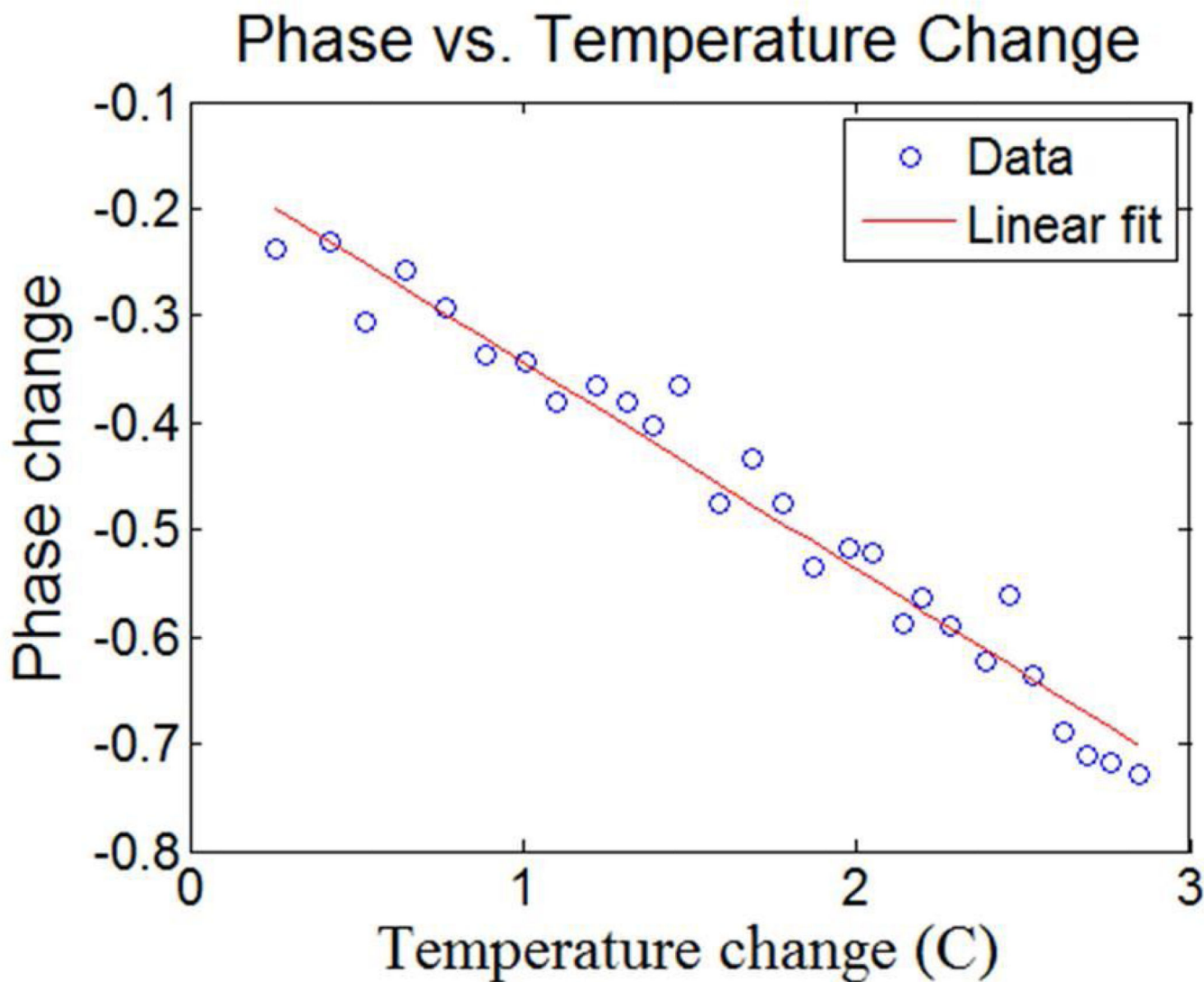
Figure 1.
Medium temperature will change the procession speed of the hydrogen atom. The procession speed of the hydrogen atom is linear proportion to the temperature. As a result, the phase difference caused by the hydrogen atom procession speed difference will also be linear proportion to the medium temperature change after certain sampling time as shown in the figure. (MRI echo time, T_E.)
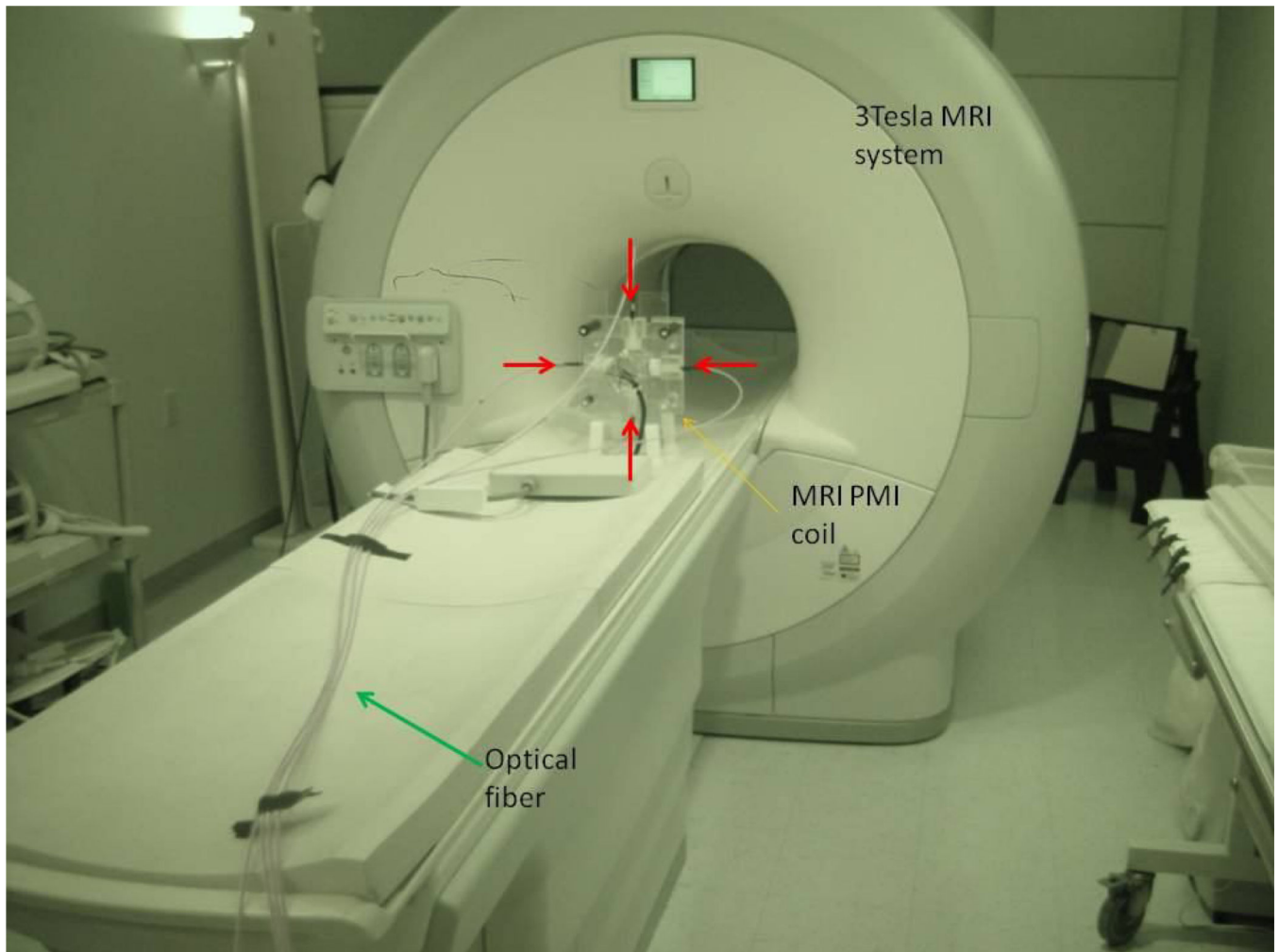
Figure 2.
shows the Photo-magnetic experiment set-up. The green arrow shows the 20 meters long, 1mm diameter optical fibers which transfer the light from MRI control room into MRI scanner room. The fibers are coupled to a specially designed MRI coil, which can illuminate the laser to the medium from four sides. (red arrows) The yellow arrow is the custom designed MRI animal coil for the PMI system.
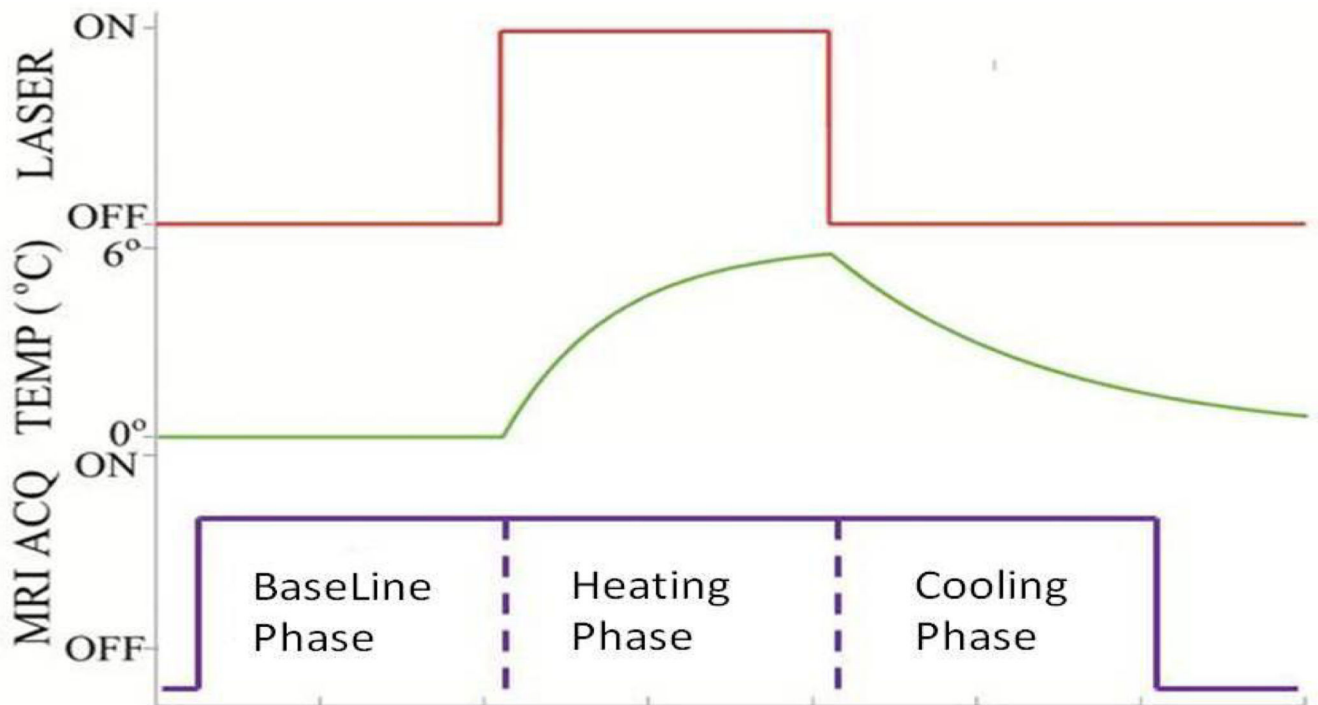
Figure 3.
The timing diagram of PMI. First we obtain the baseline MRI phase map of the object before we turn on the laser (Baseline Phase). Then we turn on the laser and measure the phase change in the MRI signal (Heating Phase). In the final step, we turn off the laser to obtain the phase signal during cooling (Cooling Phase).
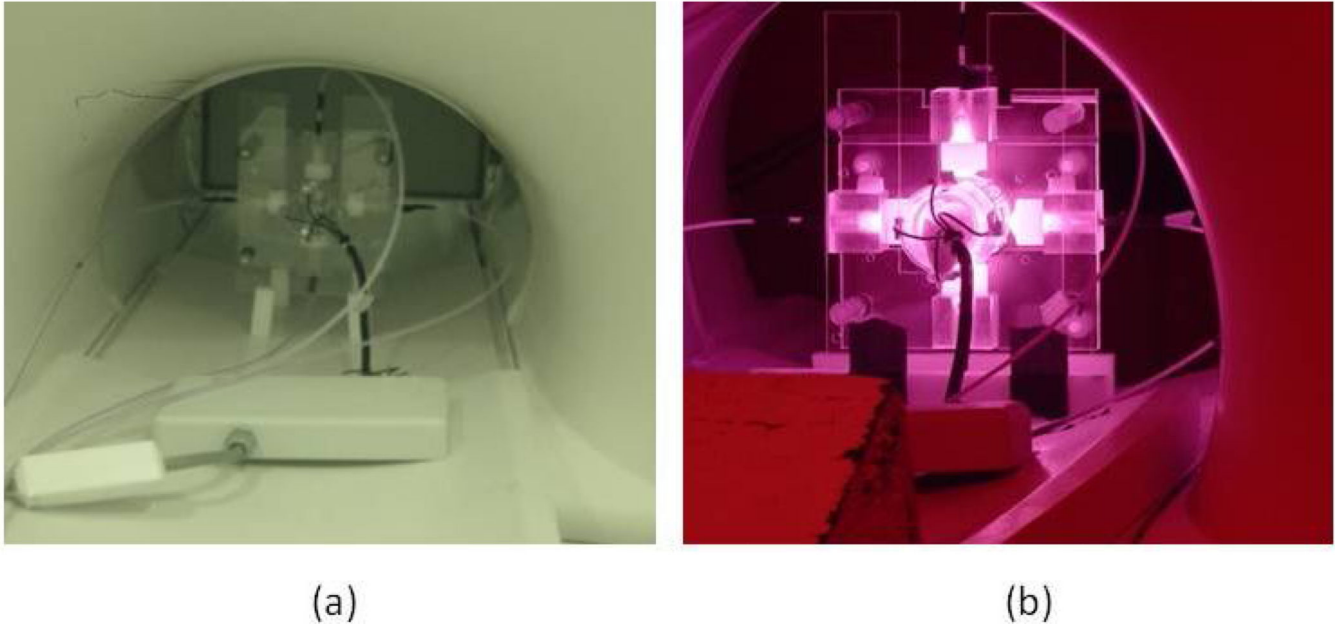
(a)

(b)

Figure 4.
(a) The PMI coil during the baseline scan.
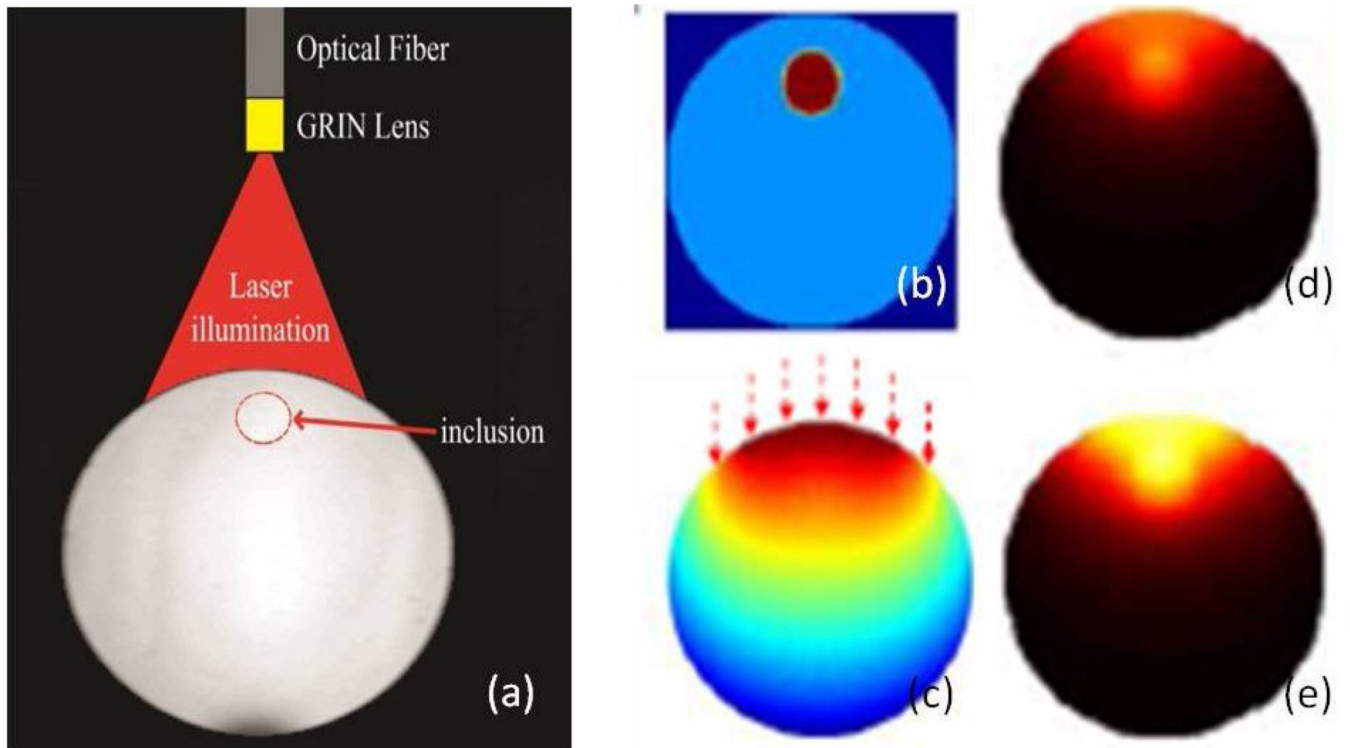(b) the laser illumination during heating phase scan - captured by a SONY night vision camera.

Figure 5.
(a) The phantom and illumination setting of the experiment.
(b) The true optical absorption map of the phantom.
(c) The simulated photon density distribution map of the experiment in log scale.
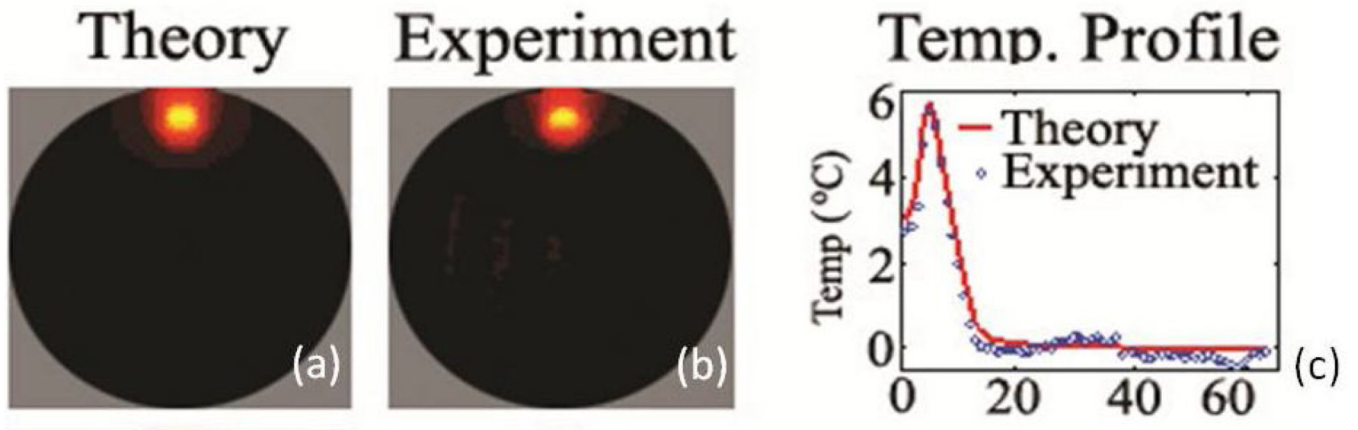(d)& (e) The temperature map measured by PRF MR thermometry with 5 and 10 seconds at laser heating step, respectively.

Figure 6.
(a) & (b) The temperature map simulated by FEM based forward solver and measured by PMI system.

(c) The profile of both temperature maps across the center of the phantom and high absorption inclusion.